Mesoscopic dynamic model of epithelial cell division with cell-cell junction effects

Zong-Yuan Liu,[1] Bo Li,[1] Zi-Long Zhao,[1] Guang-Kui Xu,[2] Xi-Qiao Feng ●,[1,*] and Huajian Gao[3,4]

[1]*Institute of Biomechanics and Medical Engineering, AML, Department of Engineering Mechanics,*
Tsinghua University, Beijing 100084, China

[2]*International Center for Applied Mechanics, State Key Laboratory for Strength and Vibration of Mechanical Structures,*
Xi'an Jiaotong University, Xi'an 710049, China

[3]*School of Mechanical and Aerospace Engineering, Nanyang Technological University, Singapore 639798, Singapore*

[4]*Institute of High Performance Computing, A*STAR, Singapore 138632, Singapore*

Cell division is central for embryonic development, tissue morphogenesis, and tumor growth. Experiments have evidenced that mitotic cell division is manipulated by the intercellular cues such as cell-cell junctions. However, it still remains unclear how these cortical-associated cues mechanically affect the mitotic spindle machinery, which determines the position and orientation of the cell division. In this paper, a mesoscopic dynamic cell division model is established to explore the integrated regulations of cortical polarity, microtubule pulling forces, cell deformability, and internal osmotic pressure. We show that the distributed pulling forces of astral microtubules play a key role in encoding the instructive cortical cues to orient and position the spindle of a dividing cell. The present model can not only predict the spindle orientation and position, but also capture the morphological evolution of cell rounding. The theoretical results agree well with relevant experiments both qualitatively and quantitatively. This work sheds light on the mechanical linkage between cell cortex and mitotic spindle, and holds potential in regulating cell division and sculpting tissue morphology.

I. INTRODUCTION

During metazoan development, epithelial tissues undergo dramatic morphogenetic evolutions to achieve their exquisite architecture [1]. The orientation and position of cell division specified by the spindle direction and location lie at the heart of regulating cell fate, orchestrating tissue architecture, and sculpting organ shape [2–6]. In most epithelial tissues, neighboring cells are mechanically linked to each other through cell-cell junctions [7–9]. These adhesive structures remain intact during the dramatic cell shape evolution in epithelial proliferation, ensuring the stable mechanical connections between cells across the whole tissue [10].

Besides maintaining the structural integrity of epithelial tissues, cell-cell junctions also provide cortical cues to orient planar cell divisions. E-cadherin regulates cell division orientation in alignment with cell-cell adhesions by forming stable cortical attachments between astral microtubules and E-cadherin-based adhesions [11]. Hart *et al.* [12] also found that E-cadherin-based cell-cell adhesion regulates cell division orientation by recruiting cortical force-generating protein complexes such as LGN and NuMA. Besides E-cadherin-based junctions, Bosveld *et al.* [13] demonstrated that tricellular junctions also play an important role in orienting the mitotic cell division. Despite the above-highlighted experimental advances, it still remains unclear how the cortical cues of cell-cell junctions are transmitted into the spindle

orientation machinery to steer division orientation along with other influencing factors.

In this work, we establish a mesoscopic dynamic cell division model to address the above issue. The model takes into account the cortical concentration of LGN-NuMA and dynein complexes, microtubule pulling forces, cell rounding pressure, cell deformability, and tissue viscoelasticity. LGN-NuMA and dynein are the cortical force-generating complexes, which determine the spindle orientation by pulling on astral microtubules [14–17]. The present model aims to capture the biomechanical mechanisms underpinning the signal transmission during the mitotic cell division. We demonstrate that the distributed microtubule pulling forces regulated by the cortical LGN-NuMA and dynein concentration can transmit the biochemical signals of intercellular junctions into the biomechanical signals received by the mitotic spindle. Our findings provide insights into the biophysical basis of relevant experimental phenomena [11–13] in cellular mechanosensing systems.

II. MODEL AND METHODS

Predicting the position and orientation of the cell division plane remains a fundamental issue in the cell and developmental biology. Théry *et al.* [18] proposed a steady-state model to predict the spindle orientation of adhesive cells spreading on micropatterns, providing a mechanical explanation for how cells sense their long axis. This model has also been used to explain the influence of cell geometry on cell division in sea urchin embryos [19]. Zhao *et al.* [20] investigated the dynamics of a single cell confined in microchambers, and

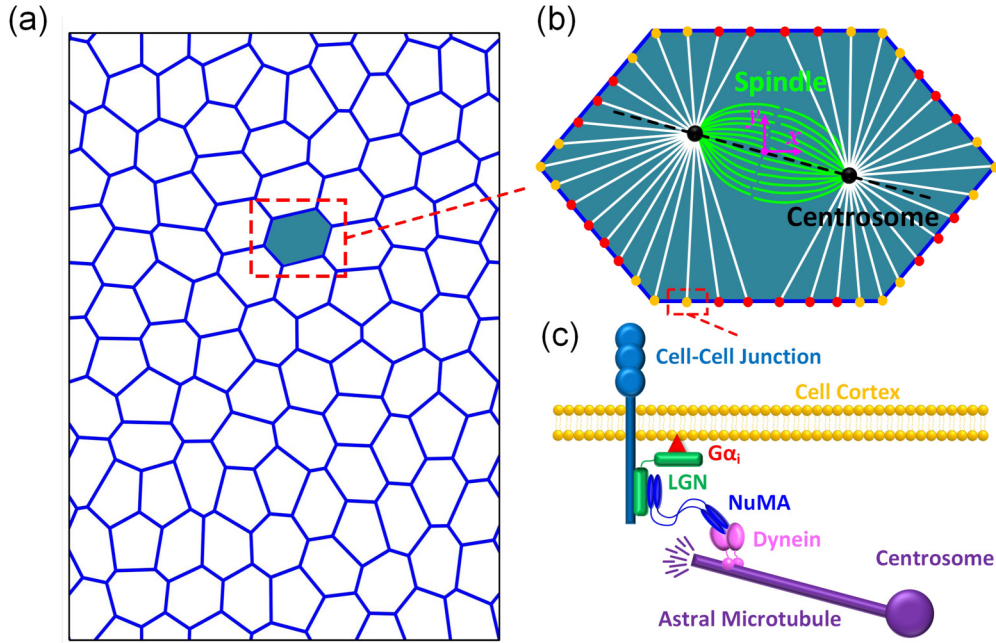*Corresponding author: fengxq@tsinghua.edu.cn

FIG. 1. Schematic of the dynamic mesoscopic cell division model. (a) The classical polygonal cell packing geometry of epithelial tissues. (b) The representative dividing epithelial cell. Cell cortex is characterized by the cortical joints. The cortical joints with high LGN-NuMA and dynein concentration are illustrated in yellow, and those with low LGN-NuMA and dynein concentration are in red. The spindle orientation is characterized by the acute angle between the x axis and the spindle axis defined by the two centrosomes. (c) Schematic of the LGN-NuMA and dynein dominated microtubule-cortex connections.

revealed that the position and orientation of the cell division plane are highly affected by boundary confinements. Besides the geometric effects, intercellular cues such as cell-cell junctions also contribute to the mitotic spindle orientation [21]. By comparing the polarity-based cell division model with the classical shape-based cell division model, Bosveld *et al.* [13] found that the orientation of cell division is defined by the tricellular junctions. In spite of the previous theoretical efforts, there still lacks an inclusive dynamic model that can predict both the position and orientation of cell division with the effects of cell deformation and cell polarity.

We investigate the spatiotemporal evolution of mitotic cells in a growing epithelial monolayer [Fig. 1(a)]. In a simple description of epithelia, the cells usually divide in the plane of the monolayer [2]. During the division of a cell, its essential structural components, such as E-cadherin and actomyosin, are approximately located in the plane of division [22,23]. Therefore, we consider a two-dimensional (2D) model by assuming that the cytoskeleton, nucleus, and cell-cell junctions are all coplanar, as in previous references [24–26]. The 2D model of a cell monolayer allows us to investigate the large deformation and dynamic behaviors of mitotic spindles while ignoring the three-dimensional deformation of the cell cortex.

In the simulations, we pay particular attention to a representative dividing cell in epithelial monolayer [27]. We assume that, at the initial state, the cell has a hexagonal shape with geometric polarity, containing the cytoskeleton and the spindle [Fig. 1(b)]. The cell shape is characterized by the cortical joints associated with LGN-NuMA and dynein complexes [Fig. 1(c)]. There are two centrosomes and a number of astral microtubules bridging the centrosomes with the cell cortex [Fig. 1(b)]. Although the mature bipolar spindle has not

yet formed at the beginning of mitosis, we assume an initial position of the spindle and the centrosomes. Each microtubule generates an axial pulling force between a centrosome and the cell cortex. The mitotic spindle is moved and torqued by the pulling forces exerted by the astral microtubules during mitosis, and its final equilibrium state dictates the position and orientation of cell division. For the sake of simplicity, we do not consider the detailed structural components of the surrounding cells, but model them as a viscoelastic medium. Thus, during the dramatic deformation of the dividing cell, the cell cortex is subjected to external viscoelastic resistance from the surrounding tissue.

The forces acting on the cell cortex and the spindle are shown in Fig. 2, and they will be calculated by solving the coupled equilibrium equations of the cell cortex and the spindle. In our simulations, we divide the cell cortex into hundreds of segments to track its morphological evolution. During mitotic cell rounding, an epithelial cell experiences dramatic changes in its area and shape. Our mesoscopic dynamic model can predict the geometric change of a cell under large deformation, even when the cell cortex deforms into a nonconvex shape [20].

A. Cortical spatial cues

LGN-NuMA and dynein are the evolutionarily conserved cortical force-generating complexes, which control spindle position and orientation by capturing and pulling on the dynamic plus ends of astral microtubules [14–17]. Recent experiments showed that during mitosis, cell-cell junctions recruit LGN-NuMA and dynein complexes, which significantly affect protein concentrations in the cell cortex [11–13]. The
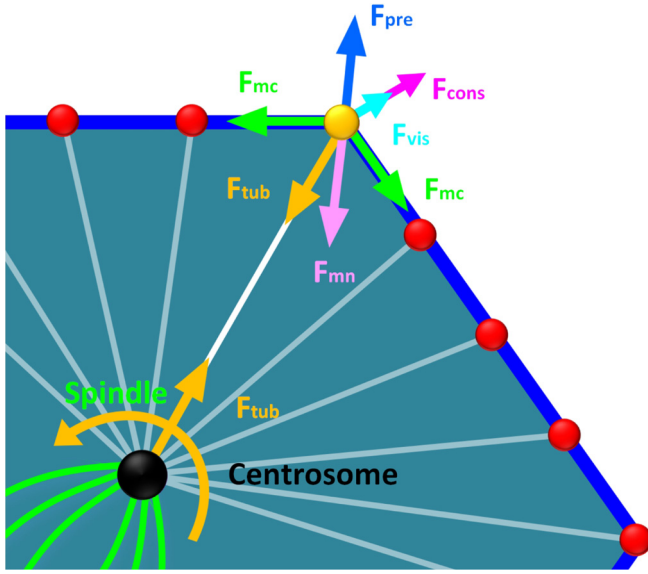
FIG. 2. Schematic of the forces and torque acting on the cell cortex and the mitotic spindle. The cortical joints with high LGN-NuMA and dynein concentration are illustrated in yellow, and those with low LGN-NuMA and dynein concentration are in red. Here, F_{tub} is the dynein-generated microtubule pulling force, F_{mc} is cortical tension along the circumferential direction, F_{mn} is the force induced by the change in cell area, F_{pre} is the internal osmotic pressure during the mitosis, F_{cons} is the constraining force induced by the elastic resistance of neighboring cells, and F_{vis} is the viscous resistance force induced by tissue viscosity.

accumulation of cortical LGN-NuMA and dynein complexes results in an increase of microtubule forces by forming stable attachments [11] and generating multiple-arm capture and pulling [28] between astral microtubules and the cell cortex. Accounting for the distributed concentration of cortical LGN-NuMA and dynein complex, we correlate, in the proposed mesoscopic cell division model, the spindle positioning and orientation with cell-cell junctions. In this way, the intercellular spatial cues induced by cell-cell junctions can be transmitted into spindle orientation machinery to regulate the cell divisions.

In LGN-NuMA and dynein complexes, dynein acts as molecular motors, binding cortex adaptor protein NuMA with astral microtubules [3,13,17] and generates a pulling force on astral microtubules through hydrolyzing ATP [29]. The mechanical behavior of astral microtubules varies with the concentration of cortical LGN-NuMA and dynein complexes [13,16]. The pulling force of a microtubule is approximately proportional to the LGN-NuMA and dynein concentration and can be expressed as [30,31]

$$F_{\text{tub}} = N F_0 \left(1 - \frac{v}{v_0} \right) r_{\text{tub}}, \tag{1}$$

where N denotes the relative concentration of LGN-NuMA and dynein complexes in the cell cortex compared with that in cytoplasm, which can be estimated by the experimentally measured ratio between the cortical and cytoplasmic protein fluorescence intensities [11–13]; $F_0 = 5\,\text{pN}$ is the stall force, $v_0 = 0.2\,\mu\text{m/s}$ is the unloaded velocity of dynein, and v is the

velocity magnitude of the dynein anchored in the cell cortex; r_{tub} denotes the unit vector pointing from the cortical joint to the centrosome.

B. Cellular stiffness

During mitosis, epithelial cells undergo large deformation, which induces resistance forces simultaneously. It has been found that the mitotic cortex becomes more rigid than the interphase cortex, increasing the stiffness of mitotic cells [32–34]. The cortical tension associated with cell deformation affects the cell shape to a large extent [25] and cannot be ignored. We describe the cortical tension F_{mc} along the circumferential direction by

$$F_{\text{mc}}^+ = K_{\text{L}} s^+, \quad F_{\text{mc}}^- = K_{\text{L}} s^-, \tag{2}$$

where the line tension $K_{\text{L}} = 0.002\,\text{N/m}$ along the cell cortex is induced by actomyosin contractility [26,27]. s^+ denotes the vector pointing from cortical joint i to $i + 1$, and s^- the vector pointing from cortical joint i to $i - 1$.

Besides the cortical tension, the cell areal stiffness also affects the epithelial cell deformation [24,26,27]. The areal stiffness induced force F_{mn} in the direction perpendicular to the cell cortex is described by

$$F_{\text{mn}} = -K_a \hat{s}(A - A_0) r_{\text{nor}}, \tag{3}$$

where $\hat{s} = (|s^+| + |s^-|)/2$; $K_a = 5\,\text{pN}\,\mu\text{m}^{-3}$ is the areal elastic modulus [35,36]; A and A_0 denote the current and the initial cell area; $r_{\text{nor}} = \{(s^- - s^+) \times z\}/|s^- - s^+|$ is the unit vector normal to the local cell cortex [37], with z being the unit vector normal to the epithelial plane.

C. Osmotic pressure

During mitosis, the forces generated by the internal osmotic pressure help the cell to push their surroundings to round up [38]. The epithelial monolayers have a typical cell height of $H \sim 5\,\mu\text{m}$ [39,40]. During the deformation of the cell, the internal osmotic pressure always pushes the cell cortex outward, generating forces along the normal direction r_{nor} at the local cortex. The force generated by the osmotic pressure can be calculated by

$$F_{\text{pre}} = PH\hat{s} r_{\text{nor}}, \tag{4}$$

where $P = 100\,\text{Pa}$ is the rounding pressure [38].

D. External resistance

The dividing cell also subjects to the forces arising from intercellular connections *in vivo* [41]. In epithelia, cell deformation is affected by the contractions from neighboring cells [42,43]. In our model, therefore, we add elastic constraints to the cortex of the representative mitotic cell to mimic the stretch from the surrounding cells [44]. The constraining force induced by the elastic resistance of neighboring cells, F_{cons}, follows the Hookean law

$$F_{\text{cons}} = -k u, \tag{5}$$

where $u = x - x_0$ is the displacement of the cortical joint, with x and x_0 being the current and initial positions, respectively. Here we take the effective spring constant $k =$

0.002 N/m, according to the elasticity measurements of epithelial tissues [45].

We also consider a viscous resistance force arising from the viscosity of the surrounding tissue. The viscous resistance force depends on not only the composite shell envelopes of the neighboring cells, but also their internal cytoskeleton and the intercellular junctions [46,47]. The viscous resistance force acting on the cortex is written as

$$\boldsymbol{F}_{\text{vis}} = -\hat{s}\eta_{\text{c}}\boldsymbol{v}, \tag{6}$$

where $\eta_{\text{c}} = 10^4$ Pa s denotes the tissue viscosity [48], $\boldsymbol{v} = d\boldsymbol{x}/dt$ is the velocity of the cell cortex.

E. Thermal fluctuations

Gaussian white noise arising from fluctuations is introduced via a random force $\boldsymbol{F}_{\text{noise}}$ acting on the cell cortex,

$$\boldsymbol{F}_{\text{noise}} = F_{\text{R}}\boldsymbol{r}_{\text{noise}}, \tag{7}$$

where $\boldsymbol{r}_{\text{noise}}$ is the unit-variance Gaussian noise vector at the cell cortex, and F_{R} is the intensity of white noise. The main results of our simulations on the spindle orientation and positioning, as well as cell rounding, are not affected by the random force $\boldsymbol{F}_{\text{noise}}$ with magnitude ranging from 10 pN − 200 pN, according to previous studies [49–52]. In our study, we take $F_{\text{R}} = 100$ pN [52].

F. Simulation method

Following the above analysis, the mechanical equilibrium condition of the microtubule-cortex joint i is written as

$$N F_0\left(1 - \left|\frac{d\boldsymbol{x}_i}{v_0 dt}\right|\right)\boldsymbol{r}^i_{\text{tub}} + K_{\text{L}}\boldsymbol{s}_i^+ + K_{\text{L}}\boldsymbol{s}_i^- - K_a\hat{s}_i(A - A_0)\boldsymbol{r}^i_{\text{nor}}$$

$$+ PH\hat{s}_i\boldsymbol{r}^i_{\text{nor}} - kd\boldsymbol{x}_i - \hat{s}_i\eta_{\text{c}}\frac{d\boldsymbol{x}_i}{dt} + F_{\text{R}}\boldsymbol{r}^i_{\text{noise}} = \boldsymbol{0}. \tag{8}$$

The equilibrium state of the spindle dictating the final division orientation and position of the cell is also required. All microtubules transfer their axial forces to the centrosomes, producing a pulling force on its spindle attachment site and a torque at the spindle center. Since the centrosomes are much smaller in size than the cell itself, they are assumed to be circular in shape with negligible deformation. The force and momentum balance equations of the spindle are formulated as

$$\sum N_i F_0\left(1 - \left|\frac{d\boldsymbol{x}_i}{v_0 dt}\right|\right)\boldsymbol{r}^i_{\text{tub}} + \boldsymbol{f} = \boldsymbol{0}, \tag{9}$$

$$\sum N_i F_0\left(1 - \left|\frac{d\boldsymbol{x}_i}{v_0 dt}\right|\right)\left(\boldsymbol{r}_{\text{cen}} \times \boldsymbol{r}^i_{\text{tub}}\right) + \boldsymbol{\tau} = \boldsymbol{0}, \tag{10}$$

where $\boldsymbol{r}_{\text{cen}}$ is the vector pointing from the spindle center to the relevant centrosome, $\boldsymbol{f}$ and $\boldsymbol{\tau}$ are the viscous drag force and the viscous drag torque acting on the spindle, respectively. The viscous drag force is calculated by the Stokes law, $\boldsymbol{f} = -6\pi R\eta_p\boldsymbol{v}_s$, where $R = 5\,\mu$m is the characteristic radius of mitotic spindle [13,28], and $\boldsymbol{v}_s = \dot{\boldsymbol{X}}$ is the spindle velocity, $\boldsymbol{X}$ being the position of the spindle center. The viscous drag torque is taken as $\boldsymbol{\tau} = -\pi\eta_p R^2 H\boldsymbol{\omega}_s$ [53], where $\boldsymbol{\omega}_s = \dot{\alpha}$ is the angular velocity of the spindle, and α refers to the acute angle between the x axis and the spindle axis defined by the two

TABLE I. Parameters and their values used in the simulation.

Parameters	Value	References
Stall force of dynein F_0	5 pN	[30,31]
Unloaded velocity of dynein v_0	0.2 μm/s	[30,31]
Cortical tension K_{L}	0.002 N/m	[26,27]
Cellular area stiffness K_a	5 pNμm^{-3}	[35,36]
Rounding pressure P	100 Pa	[38]
Cell height H	5 μm	[39,40]
Tissue elasticity k	0.002 N/m	[45]
Tissue viscosity η_{c}	10^4 Pa s	[48]
Cytoplasmic viscosity η_p	200 Pa s	[54]
Spindle radius R	5 μm	[13,28]
Fluctuation force F_{R}	100 pN	[52]

centrosomes [Fig. 1(b)]. The cytoplasmic viscosity is taken as $\eta_p = 200$ Pa s [54].

In this section, we have established a mesoscopic dynamic cell division model to predict the spindle position and orientation according to the cortical LGN-NuMA-dynein concentration. The model has taken both mechanical and biological factors into account, including the cortical tension, cellular areal stiffness, rounding pressure, dynein associated pulling forces, cortical bridging-protein concentration, tissue viscoelasticity and the constraints from neighboring cells. The governing equations of the microtubule-cortex joints and the spindle are coupled, as given in Eqs. (8)–(10). The unknown variables, including the position of the spindle center ($\boldsymbol{X}$), the vector from the spindle center to the centrosome ($\boldsymbol{r}_{\text{cen}}$), and the positions of the cortical joints ($\boldsymbol{x}_i$), can be numerically solved by finite difference method. All examples are iteratively solved for 1000 s, which is sufficiently long for the whole system to reach the steady state. While the mitotic phase of an epithelial cell may last approximately 30 min [55,56], the cell rounding process is accomplished within the first 10 min after nuclear envelope breakdown (NEB) and, thereafter, the cell keeps the spherical shape till cytokinesis [38]. Mitotic spindle tracking also suggests that after NEB, it experiences a rotation, which takes about 10–15 min to reach the stable position and orientation [57,58]. In our analysis, we simulate the cell rounding and spindle dynamics, which occur within the beginning 15–20 min of mitosis. All parameters used in the simulations are adopted from previous experimental or theoretical studies in the literature, as shown in Table I.

III. RESULTS

A. Comparison with experiments

Specific molecular modules anchored in the cell cortex, also known as cortical force-generating machinery, have been verified to guide the mitotic spindle orientation in both invertebrates and vertebrates cells [59]. Among the diverse cortical cues, the evolutionarily conserved LGN-NuMA and dynein complexes lie at the heart of regulating the mitotic spindle orientation [60]. Recent experiments evidenced that cell-cell junctions, such as E-cadherin-mediated adhesion and tricellular junctions, induce the polarized accumulation of LGN-NuMA (*Drosophila* Mud) at the cell cortex [Fig. 3(a)].
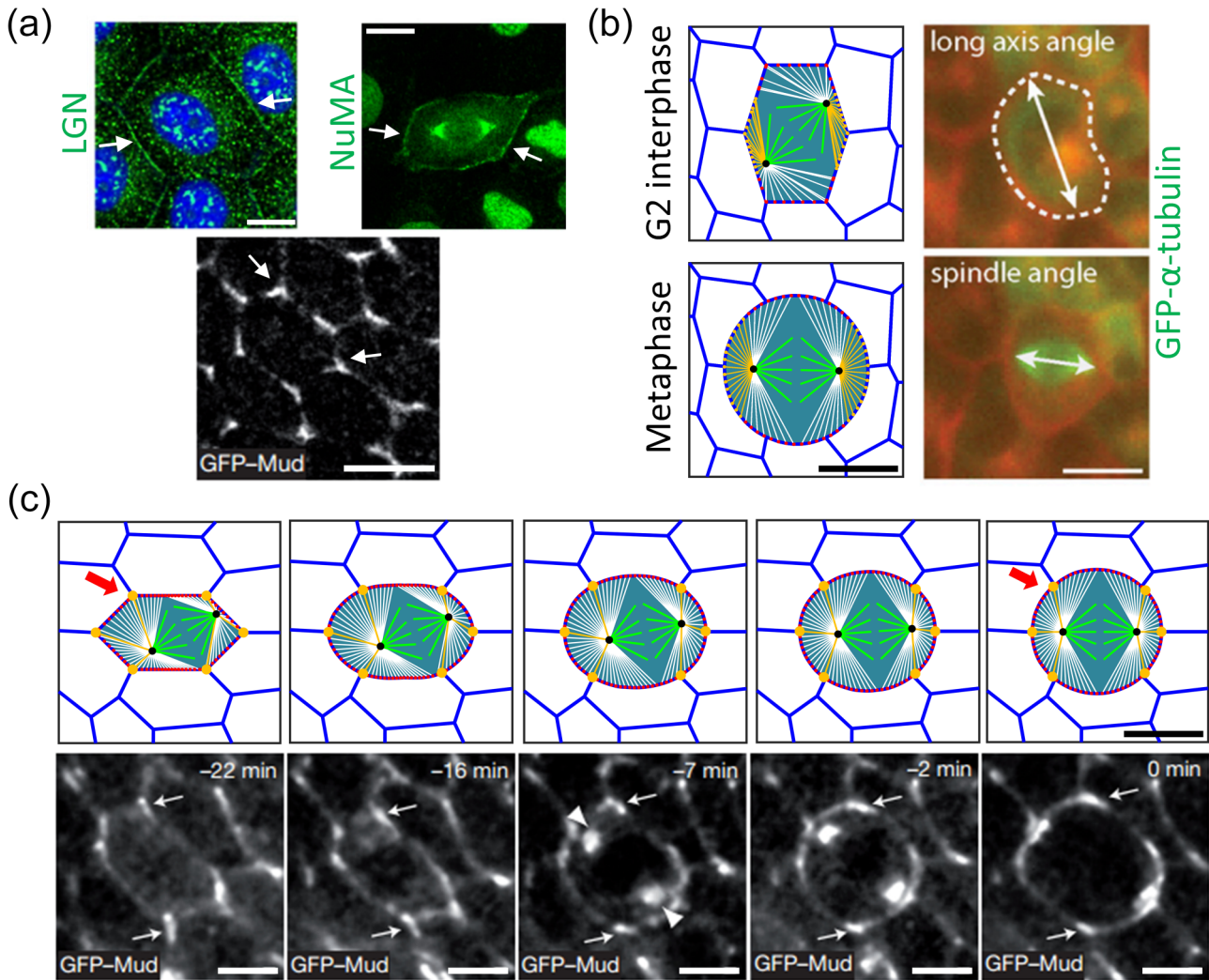
FIG. 3. (a) The polarized distributions of LGN and NuMA (white arrows) in the cell cortex (top panels, adapted from Ref. [12] with permission). NuMA's *Drosophila* homolog Mud (white arrows) enriches at the tricellular junctions (bottom panels, adapted from Ref. [13] with permission). (b) The polarized distributions of cortical cues induce the cell to divide along the interphase short axis (see also Movie 1 in the Supplemental Material [61]). The cortical joints with high LGN-NuMA and dynein concentration are illustrated in yellow, and those with low LGN-NuMA and dynein concentration are in red. The cells surrounding the dividing cell are illustrated by the polygons in blue. The right panels are adapted from Ref. [12] with permission. (c) Tricellular junctional cues ensure the cell to divide along the interphase long axis (see also Movie 2 in the Supplemental Material [61]). The red arrows in the top panels mark the cortical spatial cues in the simulation. The white arrowheads and arrows in the bottom panels point out that Mud localizes at the spindle poles and the tricellular junctions during mitotic cell rounding. The bottom panels are adapted from Ref. [13] with permission. Scale bars, 10 μm.

These accumulated proteins control the mitotic cells to divide along the proper directions [12,13]. Therefore, we reconstitute these experimentally observed cortical cues in our model and compare our simulation results with the experiments. In our simulations, both the relative concentrations of LGN-NuMA and dynein complexes are taken from the experimental measurements of fluorescent intensity. For the E-cadherin-based cortical cues, we take the relative protein concentration $N = 2.0$ [12], while for the accumulated cortical cues at the tricellular junctions, we set $N = 5.0$ [13].

As can be seen from Figs. 3(b) and 3(c), the final spindle orientations predicted by our model are in line with the corresponding experiments. We find that the polarized distribution of cortical spatial cues is sufficient to orient the mitotic spindle along the initial cell short axis, as observed in experiments

[Fig. 3(b) and Movie 1 in the Supplemental Material [61]]. Besides, the tricellular junctional cues remain intact during cell rounding, serving as the spatial landmarks on the cortex to guide the cell division along the interphase long axis [Fig. 3(c) and Movie 2 in the Supplemental Material [61]].

B. Effect of E-cadherin-based adhesion

The 136-year-old Hertwig's law states that a cell divides along the long axis of the interphase cell, which plays a profound role in tissue morphogenesis [62,63]. Recently, however, Hart *et al.* [12] demonstrated that epithelial cell divisions align with tissue tension independently of interphase cell shape and as a consequence, cells divide along their geometric short axis. In addition, the cell shape-independent
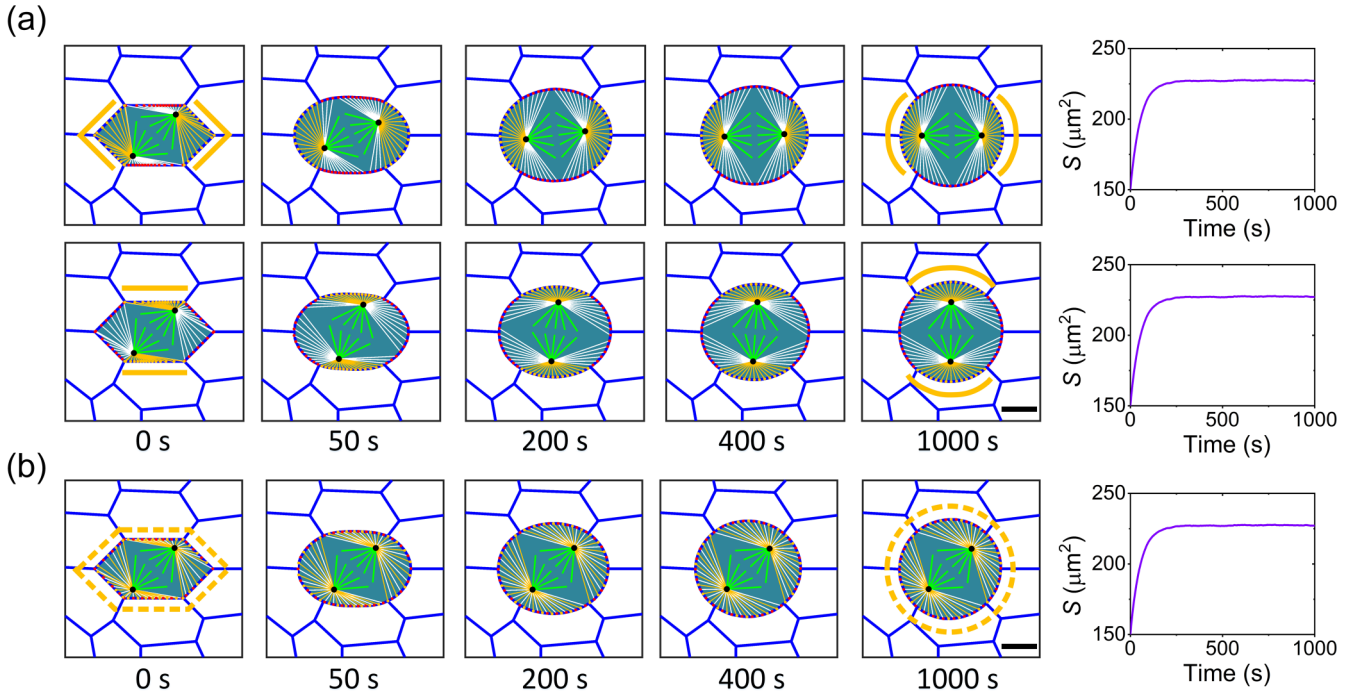
FIG. 4. Effect of E-cadherin-induced cortical cues on the mitotic spindle orientation. The cortical joints with high LGN-NuMA and dynein concentration are illustrated in yellow, and those with low LGN-NuMA and dynein concentration are in red. (a) Dynamic evolution of the cells with contrary polarity of cortical spatial cues. (b) Dynamic evolution of the cell with disrupted cortical cues. Scale bars, $5\mu m$.

divisions require the polarized recruitment of LGN-NuMA complexes to E-cadherin-based cell-cell adhesion [12]. To identify the regulatory roles of the polarized concentration of LGN-NuMA and dynein complexes induced by E-cadherin-based cell-cell adhesion, we here account for the effects of nonuniform distributed cortical spatial cues [11,12]. To elucidate the spindle orientation dynamics regulated by spatial cues, we only vary the initial concentration of the cortical proteins in different examples while the initial cell geometry, spindle position, and orientation are assumed identical. The dynamic evolutions of cells under several representative initial protein concentrations are compared in Fig. 4. In all cases the cell area approaches a constant S at last (Fig. 4, right panels), indicating that the final steady states are achieved.

Our simulations show that the E-cadherin-induced cortical spatial cues can dominate the interphase cell shape and then determine the mitotic spindle orientation. The final orientation of spindle is in consistency with the cortical spatial cues, independent of the initial cell geometry [Fig. 4(a)]. In the cells whose cortical spatial cues are distributed according to the interphase cell long axis [Fig. 4(a), top panels], which happens in the oriented cell divisions [59], the polarized cortical cues ensure that the cell division occurs along the interphase cell long axis. In addition, due to the polarized distribution of microtubule pulling forces with respect to the cortical spatial cues, cells can divide along their interphase short axis [Fig. 4(a), bottom panels], as observed in experiments [12].

Previous experiments showed that the disruption of E-cadherin-mediated adhesion without losing overall intercellular junction results in the E-cadherin and LGN protein distribute uniformly throughout the entire cell cortex and further abolishes the mitotic spindle orientation in epithelial monolayers [11,64,65]. To see how uniformly distributed cell-cell adhesion cues regulate the epithelial spindle orientation, we consider a uniform distribution of LGN-NuMA and dynein complexes in the representative cell, as observed in the experiments [11,64]. It can be seen that there is no torque acting on the mitotic spindle when the cortical spatial cues are uniformly distributed around the whole cell cortex and, consequently, the spindle orientation fails [Fig. 4(b)]. This further demonstrates that the cell-cell adhesion-induced cortical spatial cues instruct the mitotic spindle through the distributed microtubule pulling forces.

At mitosis, cells undergo a drastic shape change, during which cells gradually abandon their flattened, spread morphology and evolve into a rounded shape [66–68]. This phenomenon, known as mitotic cell rounding, appears in most eukaryotes without a rigid cell wall [63]. Our simulation shows that mitotic cells gradually attain a round shape during mitosis, irrespective of the initial LGN-NuMA-dynein complex concentration. This suggests that the cell rounding is dominated by some universal mechanisms of mitosis, such as the cortical tension and the internal osmotic pressure.

C. Effect of tricellular junctions

As a specialized type of tight junctions, tricellular junctions form at the vertices where three cells meet [69]. It has been verified that in *Drosophila* epithelia, tricellular junctions encode cellular geometry information to orient division along the interphase cell long axis. This coordination involves the participation of the dynein-associated protein Mud, which is the homolog of NuMA [13]. To explore the regulatory role of tricellular junctional cortical
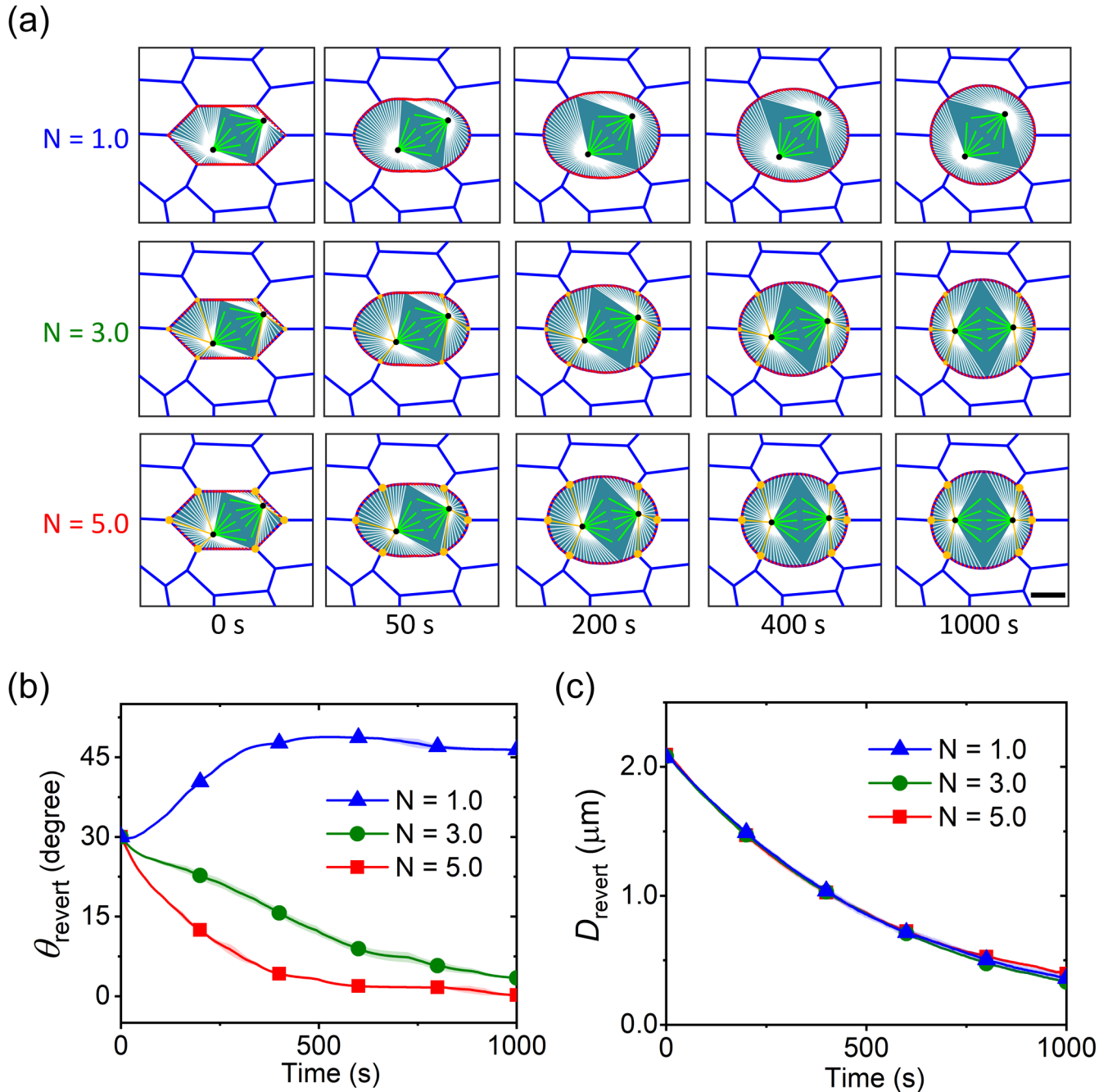
FIG. 5. Effect of tricellular junctional spatial cues on the mitotic spindle orientation and positioning. The cortical joints with high LGN-NuMA and dynein concentration are illustrated in yellow, and those with low LGN-NuMA and dynein concentration are in red. (a) Dynamic evolutions of cells with different ratios of cortical to cytoplasmic Mud concentration N at the tricellular junctions. Time evolutions of (b) reverting angle θ_{revert} and (c) reverting distance D_{revert} under different cortical to cytoplasmic Mud concentrations (mean $\pm$ std from five parallel simulations). Scale bar, 5 μm.

cues, we reconstruct the accumulated Mud concentration at the positions of tricellular junctions in the dividing cells (Fig. 5).

The simulations show that the tricellular junction-associated spatial cues are essential for the proper cell division orientation. By increasing the relative concentration of Mud at the tricellular junctions from $N = 1.0$, $N = 3.0$ to $N = 5.0$, the spindle can be rapidly oriented along the initial long axis of the cell [Figs. 5(a) and 5(b)]. To quantify the dynamic

process of mitotic spindle orienting along the initial long axis, we define the reverting angle $\theta_{\text{revert}} = \theta_{\text{spindle}} - \theta_{\text{shape}}$, where θ_{spindle} is the spindle orientation angle and θ_{shape} is the initial long axis angle of the cell. The steady magnitude of θ_{revert} under $N = 5.0$ approaches zero, indicating that the spindle aligns perfectly along the initial long axis of the cell [Fig. 5(b)]. However, the spindle deviates from the initial long axis of the cell in the example when accumulated tricellular-junctional cues are neglected ($N = 1.0$) [Fig. 5(b)].
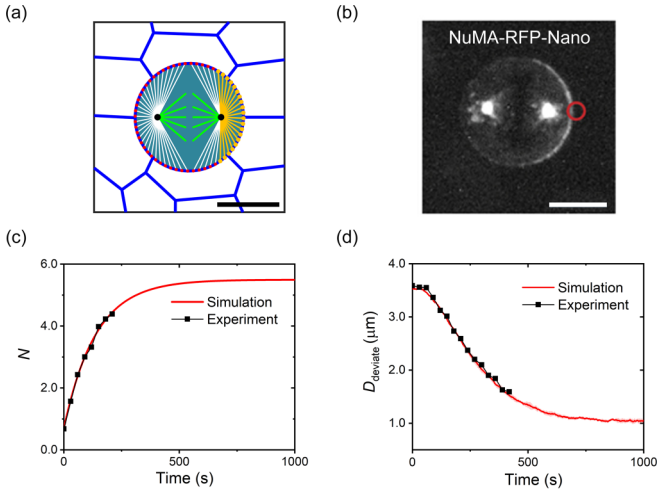
FIG. 6. Effect of asymmetric cortical cues on the mitotic spindle positioning. (a) Asymmetric cortical cues of metaphase cells in simulation. The cortical joints with high LGN-NuMA and dynein concentration are illustrated in yellow, and those with low LGN-NuMA and dynein concentration are in red. (b) Light-illumination-induced cortical accumulation of NuMA in the metaphase cells. The image is adapted from Ref. [28] with permission, where the red circle indicates the light-illuminated cortical region. (c) Cortical to cytoplasmic concentration N of NuMA at the light-illuminated cortical region. (d) The distance between the right spindle pole and the light-illuminated cell cortex D_{deviate} quantifies the spindle movement (mean $\pm$ std from five parallel simulations). The experimental data are taken from Ref. [28] with permission. Scale bars, 10μm.

In this case, the cell would not divide along the interphase long axis in the end.

Spindle positioning, together with spindle orientation, determines the placement of the cleavage plane and plays a crucial role in epithelial tissue development [70,71]. We next examine the spindle positioning process under the tricellular-junctional spatial cues. The initial position of the spindle is designedly placed at a location deviating from the cell center. We define the reverting distance D_{revert} as the distance between the spindle center and the cell center. Our calculations show that no matter whether the mitotic spindle orients along the initial cell long axis or not [Fig. 5(b)], all spindles in the considered examples eventually move to the cell center [Fig. 5(c)]. Our results suggest that the tricellular junctional cues regulate the torque that rotates the spindle, whereas the resultant force acting on the spindle determines the spindle position at the cell center.

D. Effect of asymmetric cortical cues

During the mitosis of a cell, the coupled spindle orientation and positioning process determines the final division plane synergistically [72,73]. To examine this synergetic mechanism, we introduce asymmetric distributions of cortical spatial cues in our model [Fig. 6(a)], which reconstitute the light illumination-induced cortical accumulation of NuMA-RFP-Nano in metaphase cells [28], as shown in Fig. 6(b).

In our simulations, the relative concentrations of LGN-NuMA and dynein complexes N in the light-illuminated

cortical regions are specified according to the experimental fluorescence intensity measurements [Fig. 6(c)]. We define the deviating distance D_{deviate} as the distance between the right spindle pole and the light-illuminated cell cortex. The simulation results show that with the accumulation of the cortical cues, the mitotic spindle is gradually pulled towards the light-illuminated cortical regions [Fig. 6(d)], whereas the spindle orientation is not significantly affected. These results indicate that the resultant force acting on the mitotic spindle determines the final division plane, and the asymmetric distribution of cortical spatial cues is responsible for the spindle resultant force towards the light-illuminated cortical regions, but the induced torque is negligibly small and cannot rotate the mitotic spindle. Our simulation results are in good agreement with relevant experimental measurements, both qualitatively and quantitatively [28].

E. Cell division adhered to E-cadherin-coated sidewalls

To further illustrate the application of our model, we consider the division of a cell adhered to E-cadherin-coated sidewalls as boundary constraints [11,74]. Previous experiments showed that the attachment between the cell and such an adhesive sidewall results in significant recruitment of LGN at the cell-sidewall contact cortical regions and biases the mitotic spindle perpendicular to the sidewall [11].

Simulations based on our cell division model show that the model can predict the mitotic spindle position and orientation under different adhesive geometrical constraints. A few examples are shown in Fig. 7. Due to the attachment between the cell cortex and the adhesive boundary, LGN-NuMA and dynein complexes are recruited in the contact cortical regions [11]. Thus, the cortical spatial cues formed at the cell–sidewall interfaces affect the resultant torque and force on the mitotic spindle. The examples in Fig. 7 demonstrate that our model can not only explain various cell division phenomena observed in cell monolayers but also account for the effects of boundary constraints. In the case when a cell adheres to a straight E-cadherin-coated wall boundary, our model predicts that its mitotic spindle tends to rotate toward the direction normal to the wall [Fig. 7(a)], in agreement with experimental observations [11].

IV. DISCUSSIONS

During the development of exquisite tissue architecture, epithelial cells rely on the instructive signals from cellular microenvironments to coordinate cell division. Previous works have shown that intercellular junctions regulate the cell division orientation through the cortical spatial cues associated with LGN-NuMA and dynein complexes [11–13]. In this work, we have proposed a dynamic cell division model integrating both cell deformation and cell polarity to unravel how the intercellular spatial cues affect the orientation and position of cell division. Our analysis shows that the astral microtubules and their distributed pulling forces are two key elements that transmit the intercellular junctional cues into the mitotic spindle. After the cortical spatial cues are established, the mitotic spindle follows the mechanical regulation based on the cortical cues to determine the final division orienta-
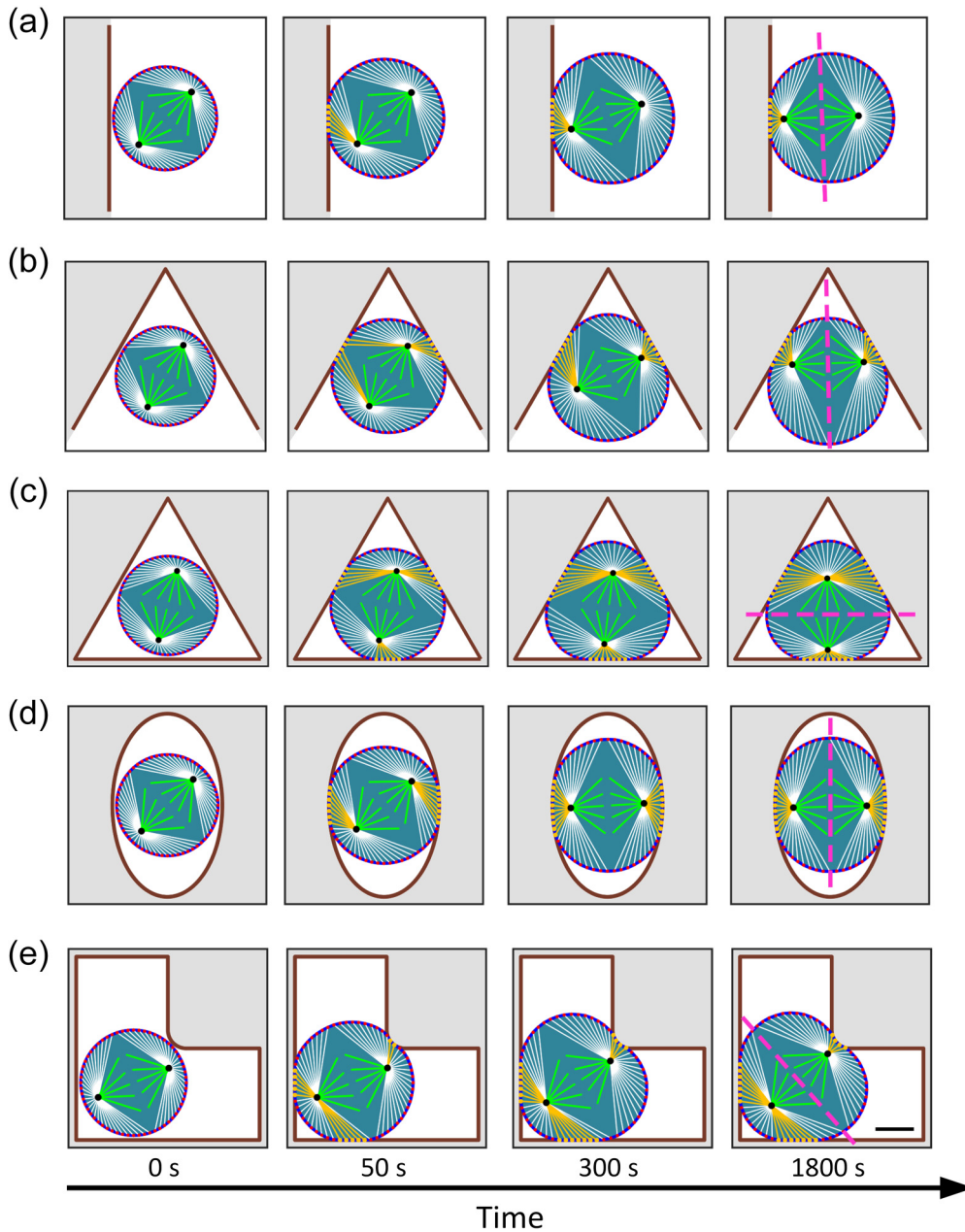
FIG. 7. Mitotic spindle orientation and positioning dynamics of cells adhered to E-cadherin-coated sidewalls: (a) a single straight wall, (b) two angular walls, (c) triangular walls, (d) elliptical walls, and (e) L-shaped walls. The dashed pink lines in last column indicate the cell division plane. The cortical joints with high LGN-NuMA and dynein concentration are illustrated in yellow, and those with low LGN-NuMA and dynein concentration are in red. Scale bar, 5μm.

tion and position. The mechanical linkage between the cell cortex and the spindle is accomplished by astral microtubules with the help of LGN-NuMA and dynein complexes [12,13]. Our results suggest that the mitotic spindle can sense and respond to cellular microenvironmental signals such as the cell-cell junctions through the mechanical linkage between centrosomes, astral microtubules and the cell cortex.

Growing evidence suggests that cell rounding is essential for the proper orientation and position of the spindle in a mitotic cell [75]. Cell rounding allows the spindle to accurately locate the cell center with the help of pulling forces of the astral microtubules [76]. Besides, the instructive cortical spatial cues are kept intact when a cell rounds up, ensuring

the cell to retain a memory of its interphase shape to orient the division axis [13,55]. In this work, we have investigated this dynamic process by integrating the spindle orientation, spindle positioning, and mitotic cell rounding. We find that mitotic cells abandon the geometrical polarity during cell rounding and, thereafter, cortical cues serve as spatial landmarks to orient the spindle [Figs. 3 and 4(a)].

Our simulations show that the torque and the resultant force acting on the spindle drive work cooperatively to control the orientation and position of cell division. During the mitosis of a cell, the two processes (orienting and positioning) may happen simultaneously (Figs. 5 and 7) or in a sequential manner (Figs. 4 and 6), depending on the pulling

force distributions in the microtubules. The concentrations of cortical LGN-NuMA-dynein dictate the microtubule pulling forces, generating a resultant force and a torque that drive the spindle to move and rotate, respectively. This mechanism helps explain the experimental observations that the mitotic spindle may evolve to different positions and directions under different conditions [77,78].

In the recent years, much effort has been devoted toward predicting the positioning and orientation of the mitotic spindle. However, most previous studies focused on predicting the final steady state of the spindle [21]. It has been recognized that the mitotic spindle moves and rotates before the final division axis is determined. These dynamic processes are especially important in the situations when the division plane needs to be precisely tuned [79]. In our model, a time scale has been introduced to explore the dynamic features of these movements. It is found that the spindle orientation and the deformation of cell cortex happen almost simultaneously and interact with each other. Our theoretical prediction for the final steady orientation of the mitotic spindle is in consistency with relevant experiments [12,13].

In 1884, Hertwig proposed the famous long axis rule, which underscores the role of cellular geometry in cell division orientation [62]. Though this geometry-based rule works well in many situations, recent experiments indicated a requirement for additional physical mechanisms built on the existence of specific polarity cues [60]. These polarized cortical proteins are maintained by protein sorting from intracellular compartments and selective retention in the membrane [80]. Besides the LGN-NuMA and dynein complexes acting as the key regulator in the spindle orientation, there are other pathways involved in recruiting force generators at the cell cortex to orient the division. For example, the actin-binding proteins ezrin-radixin-moesin (ERM) regulate the mitotic spindle orientation through organizing the F-actin meshwork beneath the cell cortex [81,82]. These additional mechanisms of orienting the mitotic spindle may also be important in some specialized epithelia and are worth further studies.

Though a dividing cell does not have a mature bipolar spindle in the G2 interphase, the polarized distribution of cortical cues has already been achieved [12,13]. To examine the combined effects of continuous cell rounding and preestablished cortical cues on the spindle dynamics, we assume an initial spindle position and orientation at the beginning of our simulation. Previous experiments showed that the mitotic spindle orientation can rotate 30–50 degrees before the final configuration is attained [57,58]. In our simulations, the initial spindle orientation from 30–45 degrees is set according to the above-mentioned experimental observations. The bipolar spindle formation, which happens at the interphase-prophase

transition, has not been considered in the current model. Centrosome separation and bipolar spindle assembly, which involve complex and multifaceted regulations of microtubule kinetics, actin association, and chromokinesins [83,84], deserve further specific study.

V. CONCLUSIONS

In summary, we have established a dynamic cell division model on the basis of biophysical mechanisms, including cortical force-generating machinery, astral microtubules, cellular stiffness, internal osmotic pressure, and cell-cell interactions. This model reveals the mechanical regulation of intercellular junctions on cell division behind the biochemical mechanisms. We find that the different concentration of the cortical cues controls the orientation and position of the mitotic spindle by coordinating the astral microtubule pulling forces. Through the mechanical linkage between the cell cortex and the mitotic spindle, the cortical signals of cell-cell junctions can be transmitted into the mitotic spindle to steer the final orientation of cell division. Moreover, we have analyzed the dynamic evolutions of the mitotic cell rounding. It turns out that the preestablished cortical spatial cues are essential for a rounded dividing cell to achieve proper spindle orientation and position. Our theoretical results can explain many important phenomena observed in relevant experiments of cell division both qualitatively and quantitatively.

Finally, it is worth emphasizing that, besides the mechanical and chemical mechanisms included in the present model, there are some other factors that may affect the dynamics of cell division. In the present model, for example, we have not accounted for the details of mechanobiological signaling pathways and multiple cell-cell, cell-substrate interactions. Our attention has been focused on a representative dividing cell, and the influences of the surrounding cells have been represented as external viscoelastic resistance to cell deformation. Improving the present model to simultaneously simulate the structural evolution of multiple cells in a monolayer is a topic for future research.

[1] C. C. Wang, L. Jamal, and K. A. Janes, Wires. Syst. Biol. Med. **4**, 51 (2012).

[2] K. Ragkousi and M. C. Gibson, J. Cell Biol. **207**, 181 (2014).

[3] T. E. Gillies and C. Cabernard, Curr. Biol. **21**, R599 (2011).

[4] J. A. Knoblich, Nature Rev. Mol. Cell Bio. **11**, 849 (2010).

[5] T. Lechler and E. Fuchs, Nature (London) **437**, 275 (2005).

[6] S. E. Williams and E. Fuchs, Curr. Opin. Cell Biol. **25**, 749 (2013).

[7] B. M. Gumbiner, Cell **84**, 345 (1996).

[8] D. G. Drubin and W. J. Nelson, Cell **84**, 335 (1996).

[9] V. Vasioukhin, C. Bauer, M. Yin, and E. Fuchs, Cell **100**, 209 (2000).

[10] T. Higashi, T. R. Arnold, R. E. Stephenson, K. M. Dinshaw, and A. L. Miller, Curr. Biol. **26**, 1829 (2016).

[11] M. Gloerich, J. M. Bianchini, K. A. Siemers, D. J. Cohen, and W. J. Nelson, Nature Commun. **8**, 13996 (2017).

[12] K. C. Hart, J. Tan, K. A. Siemers, J. Y. Sim, B. L. Pruitt, W. J. Nelson, and M. Gloerich, Proc. Natl. Acad. Sci. USA **114**, E5845 (2017).

[13] F. Bosveld *et al.*, Nature (London) **530**, 495 (2016).

[14] L. Seldin, A. Muroyama, and T. Lechler, eLife **5**, E12504 (2016).

[15] A. G. Hendricks, J. E. Lazarus, E. Perlson, M. K. Gardner, D. J. Odde, Y. E. Goldman, and E. L. F. Holzbaur, Curr. Biol. **22**, 632 (2012).

[16] L. Laan *et al.*, Cell **148**, 502 (2012).

[17] Q. S. Du and I. G. Macara, Cell **119**, 503 (2004).

[18] M. Thery, A. Jimenez-Dalmaroni, V. Racine, M. Bornens, and F. Julicher, Nature (London) **447**, 493 (2007).

[19] N. Minc, D. Burgess, and F. Chang, Cell **144**, 414 (2011).

[20] Z. L. Zhao, Z. Y. Liu, J. Du, G. K. Xu, and X. Q. Feng, Biophys. J. **112**, 2377 (2017).

[21] N. Minc and M. Piel, Trends Cell Biol. **22**, 193 (2012).

[22] N. Ramkumar and B. Baum, Nature Rev. Mol. Cell Biol. **17**, 511 (2016).

[23] A. Nematbakhsh, W. Sun, P. A. Brodskiy, A. Amiri, C. Narciso, Z. Xu, J. J. Zartman, and M. Alber, PLoS Comput. Biol. **13**, e1005533 (2017).

[24] T. Nagai and H. Honda, Philos. Mag. B **81**, 699 (2001).

[25] T. Lecuit and P. F. Lenne, Nature Rev. Mol. Cell Bio. **8**, 633 (2007).

[26] A. G. Fletcher, M. Osterfield, R. E. Baker, and S. Y. Shvartsman, Biophys. J. **106**, 2291 (2014).

[27] R. Farhadifar, J. C. Roper, B. Algouy, S. Eaton, and F. Julicher, Curr. Biol. **17**, 2095 (2007).

[28] M. Okumura, T. Natsume, M. T. Kanemaki, and T. Kiyomitsu, eLife **7**, E36559 (2018).

[29] G. Civelekoglu-Scholey, D. J. Sharp, A. Mogilner, and J. M. Scholey, Biophys. J. **90**, 3966 (2006).

[30] K. Svoboda and S. M. Block, Cell **77**, 773 (1994).

[31] S. J. King and T. A. Schroer, Nature Cell Biol. **2**, 20 (2000).

[32] Y. L. Fan, H. C. Zhao, B. Li, Z. L. Zhao, and X. Q. Feng, ACS Biomater. Sci. Eng. **5**, 3788 (2019).

[33] A. S. Maddox and K. Burridge, J. Cell Biol. **160**, 255 (2003).

[34] P. Kunda, A. E. Pelling, T. Liu, and B. Baum, Curr. Biol. **18**, 91 (2008).

[35] P. P. Girard, E. A. Cavalcanti-Adam, R. Kemkemer, and J. P. Spatz, Soft Matter **3**, 307 (2007).

[36] J. Solon, A. Kaya-Copur, J. Colombelli, and D. Brunner, Cell **137**, 1331 (2009).

[37] M. A. Spencer, Z. Jabeen, and D. K. Lubensky, Eur. Phys. J. E **40**, 2 (2017).

[38] M. P. Stewart, J. Helenius, Y. Toyoda, S. P. Ramanathan, D. J. Muller, and A. A. Hyman, Nature (London) **469**, 226 (2011).

[39] J. Farinas and A. S. Verkman, Biophys. J. **71**, 3511 (1996).

[40] W. Vandriessche, P. Desmet, and G. Raskin, Pflug. Arch. Eur. J. Phy. **425**, 164 (1993).

[41] C. P. Heisenberg and Y. Bellaiche, Cell **153**, 948 (2013).

[42] B. W. Lu, F. Roegiers, L. Y. Jan, and Y. N. Jan, Nature (London) **409**, 522 (2001).

[43] R. Le Borgne, Y. Bellaiche, and F. Schweisguth, Curr. Biol. **12**, 95 (2002).

[44] N. Founounou, N. Loyer, and R. Le Borgne, Dev. Cell **24**, 242 (2013).

[45] J. H. Hoh and C. A. Schoenenberger, J. Cell Sci. **107**, 1105 (1994).

[46] K. E. Kasza, F. Nakamura, S. Hu, P. Kollmannsberger, N. Bonakdar, B. Fabry, T. P. Stossel, N. Wang, and D. A. Weitz, Biophys. J. **96**, 4326 (2009).

[47] A. R. Bausch, F. Ziemann, A. A. Boulbitch, K. Jacobson, and E. Sackmann, Biophys. J. **75**, 2038 (1998).

[48] G. Forgacs, R. A. Foty, Y. Shafrir, and M. S. Steinberg, Biophys. J. **74**, 2227 (1998).

[49] S. Z. Lin, B. Li, and X. Q. Feng, Acta Mech. Sinica. **33**, 250 (2017).

[50] X. B. Yang, D. P. Bi, M. Czajkowski, M. Merkel, M. L. Manning, and M. C. Marchetti, Proc. Natl. Acad. Sci. USA **114**, 12663 (2017).

[51] F. Giavazzi, M. Paoluzzi, M. Macchi, D. P. Bi, G. Scita, M. L. Manning, R. Cerbino, and M. C. Marchetti, Soft Matter **14**, 3471 (2018).

[52] S. Z. Lin, B. Li, G. K. Xu, and X. Q. Feng, J. Biomech. **52**, 140 (2017).

[53] U. Lei, C. Y. Yang, and K. C. Wu, Appl. Phys. Lett. **89**, 181908 (2006).

[54] A. R. Bausch, W. Moller, and E. Sackmann, Biophys. J. **76**, 573 (1999).

[55] W. T. Gibson, J. H. Veldhuis, B. Rubinstein, H. N. Cartwright, N. Perrimon, G. W. Brodland, R. Nagpal, and M. C. Gibson, Cell **144**, 427 (2011).

[56] T. P. Wyatt, A. R. Harris, M. Lam, Q. Cheng, J. Bellis, A. Dimitracopoulos, A. J. Kabla, G. T. Charras, and B. Baum, Proc. Natl. Acad. Sci. USA **112**, 5726 (2015).

[57] M. E. Larson and W. M. Bement, Mol. Biology Cell **28**, 746 (2017).

[58] E. Peyre, F. Jaouen, M. Saadaoui, L. Haren, A. Merdes, P. Durbec, and X. Morin, J. Cell Biol. **193**, 141 (2011).

[59] X. Morin and Y. Bellaiche, Dev. Cell **21**, 102 (2011).

[60] F. di Pietro, A. Echard, and X. Morin, EMBO Rep. **17**, 1106 (2016).

[61] See Supplemental Material at http://link.aps.org/Supplemental/10.1103/PhysRevE.102.012405 for dynamic evolutions of mitotic epithelial cells.

[62] O. Hertwig, Z. Naturwiss. **18**, 175 (1884).

[63] C. Cadart, E. Zlotek-Zlotkiewicz, M. Le Berre, M. Piel, and H. K. Matthews, Dev. Cell **29**, 159 (2014).

[64] M. Inaba, H. Yuan, V. Salzmann, M. T. Fuller, and Y. M. Yamashita, PLoS ONE **5**, e12473 (2010).

[65] N. den Elzen, C. V. Buttery, M. P. Maddugoda, G. Ren, and A. S. Yap, Mol. Biol. Cell **20**, 3740 (2009).

[66] A. Harris, Dev. Biol. **35**, 97 (1973).

[67] L. P. Cramer and T. J. Mitchison, Mol. Biol. Cell **8**, 109 (1997).

[68] J. E. Aubin, K. Weber, and M. Osborn, Exp. Cell Res. **124**, 93 (1979).

[69] J. Ikenouchi, M. Furuse, K. Furuse, H. Sasaki, S. Tsukita, and S. Tsukita, J. Cell Biol. **171**, 939 (2005).

[70] S. W. Grill and A. A. Hyman, Dev. Cell **8**, 461 (2005).

[71] S. Kotak and P. Gonczy, Curr. Opin. Cell Biol. **25**, 741 (2013).

[72] C. G. Pearson and K. Bloom, Nature Rev. Mol. Cell Bio. **5**, 481 (2004).

[73] K. H. Siller and C. Q. Doe, Nature Cell Biol. **11**, 365 (2009).

[74] D. J. Cohen, M. Gloerich, and W. J. Nelson, Proc. Natl. Acad. Sci. USA **113**, 14698 (2016).

[75] M. Thery and M. Bornens, Curr. Opin. Cell Biol. **18**, 648 (2006).

[76] E. S. Collins, S. K. Balchand, J. L. Faraci, P. Wadsworth, and W. L. Lee, Mol. Biol. Cell **23**, 3380 (2012).

[77] A. Nestor-Bergmann, G. Goddard, and S. Woolner, Semin. Cell Dev. Biol. **34**, 133 (2014).

[78] T. Shinar, M. Mana, F. Piano, and M. J. Shelley, Proc. Natl. Acad. Sci. USA **108**, 10508 (2011).

[79] X. Morin, F. Jaouen, and P. Durbec, Nature Neurosci. **10**, 1440 (2007).

[80] C. Yeaman, K. K. Grindstaff, and W. J. Nelson, Physiol. Rev. **79**, 73 (1999).

[81] M. Machicoane, C. A. de Frutos, J. Fink, M. Rocancourt, Y. Lombardi, S. Garel, M. Piel, and A. Echard, J. Cell Biol. **205**, 791 (2014).

[82] S. Solinet, K. Mahmud, S. F. Stewman, K. Ben El Kadhi, B. Decelle, L. Talje, A. Ma, B. H. Kwok, and S. Carreno, J. Cell Biol. **202**, 251 (2013).

[83] S. L. Prosser and L. Pelletier, Nature Rev. Mol. Cell Biol. **18**, 187 (2017).

[84] M. E. Tanenbaum and R. H. Medema, Dev. Cell **19**, 797 (2010).